

Jasmonate-mediated wound signalling promotes plant regeneration

Guifang Zhang^{1,2,9}, Fei Zhao^{1,2,9}, Lyuqin Chen^{1,2,7,8,9}, Yu Pan³, Lijun Sun³, Ning Bao⁴, Teng Zhang^{1,2}, Chun-Xiao Cui^{2,5}, Zaozao Qiu⁵, Yijing Zhang¹, Li Yang⁶ and Lin Xu^{1*}

Wounding is the first event triggering regeneration^{1–4}. However, the molecular basis of wound signalling pathways in plant regeneration is largely unclear. We previously established a method to study de novo root regeneration (DNRR) in *Arabidopsis thaliana*^{5,6}, which provides a platform for analysing wounding. During DNRR, auxin is biosynthesized after leaf detachment and promotes cell fate transition to form the root primordium^{5–7}. Here, we show that jasmonates (JAs) serve as a wound signal during DNRR. Within 2 h of leaf detachment, JA is produced in leaf explants and activates *ETHYLENE RESPONSE FACTOR109* (*ERF109*). *ERF109* upregulates *ANTHRANILATE SYNTHASE α 1* (*ASA1*)—a tryptophan biosynthesis gene in the auxin production pathway^{8–10}—dependent on the pre-deposition of *SET DOMAIN GROUP8* (*SDG8*)-mediated histone H3 lysine 36 trimethylation (*H3K36me3*)¹¹ on the *ASA1* locus. After 2 h, *ERF109* activity is inhibited by direct interaction with *JASMONATE-ZIM-DOMAIN* (*JAZ*) proteins to prevent hypersensitivity to wounding. Our results suggest that a dynamic JA wave cooperates with histone methylation to upregulate a pulse of auxin production and promote DNRR in response to wounding.

To reveal the early molecular events on wounding during de novo root regeneration (DNRR) from *Arabidopsis* leaf explants (Fig. 1a), we carried out an RNA sequencing (RNA-seq) experiment using wild-type Columbia-0 (Col-0) leaf explants before culture (that is, t_0), at 10 and 30 min after detachment, and at 1–12 h after detachment. The results showed that the upregulation of jasmonate (JA)-related genes occurred as an early response to wounding (mainly within 1 h), before the upregulation of auxin-related genes (from 2–12 h) (Fig. 1b and Supplementary Table 1). These results indicate that JA responds rapidly to wounding.

Because JA has been shown to promote adventitious root formation^{6,12–16}, we then tested whether JA serves as a wound signal to regulate auxin accumulation during DNRR. When wild-type leaf explants were treated with coronatine-*O*-methyloxime (COR-MO)—a JA receptor inhibitor¹⁷—they showed defective adventitious root production (Fig. 1c). This defect was partially rescued by the addition of 1-naphthalene acetic acid (NAA)—a synthetic auxin (Fig. 1c). After leaf detachment, free JA and its active form JA-isoleucine (JA-Ile) were not detected at t_0 , but

were quickly upregulated by 10 min (Fig. 1d). The JA-Ile level peaked at around 30 min and started to decrease afterwards (Fig. 1d). At 4 h, both JA and JA-Ile were not detected in leaf explants (Fig. 1d). Our previous data showed that the auxin level is gradually upregulated in leaf explants after 4 h⁷. Taken together, these results show that JA is able to function as a wound signal within several minutes to 2 h, and acts upstream of auxin to promote DNRR from leaf explants.

From the RNA-seq data, we identified eight clusters of genes that were upregulated or downregulated successively in response to wounding with different patterns (Fig. 1e–g, Supplementary Fig. 1 and Supplementary Table 1). For example, cluster-1 genes were upregulated within 10–30 min, then downregulated from 1 h (Fig. 1e and Supplementary Table 1); cluster-2 genes were upregulated at around 30 min to 1 h, then downregulated from 2 h (Fig. 1f and Supplementary Table 1); and cluster-3 genes were upregulated at around 30 min to 2 h, then downregulated from 4 h (Fig. 1g and Supplementary Table 1). *ETHYLENE RESPONSE FACTOR109* (*ERF109*), which encodes an AP2/ERF transcription factor, and *ANTHRANILATE SYNTHASE α 1* (*ASA1*), which encodes the enzyme that catalyses the conversion of chorismate to anthranilate (ANT) in the tryptophan biosynthesis pathway^{8,9}, were in cluster-1 and cluster-3, respectively (Fig. 1e,g). Tryptophan is the precursor of auxin biosynthesis. *ERF109* was previously shown to be a direct target of the JA signalling pathway, and *ERF109* can directly activate *ASA1* (refs. ^{9,10,18}). We confirmed direct binding of *ERF109* to the *ASA1* promoter in the leaf explant in a chromatin immunoprecipitation (ChIP) assay (Supplementary Fig. 2).

We then explored whether the JA-*ERF109*-*ASA1* pathway contributes to rooting from leaf explants. Quantitative reverse transcription PCR (qRT-PCR) analyses and the promoter reporter line *ERF109_{pro}:LUC*, in which the luciferase (LUC) reporter gene is fused downstream of the *ERF109* promoter, showed that *ERF109* was not detected in the wild-type t_0 leaf explant, but was highly upregulated predominantly in the vasculature at 10 min after leaf detachment, gradually downregulated from 30 min, and barely detectable from 2 h onwards (Fig. 2a,b). Leaf explants of *coronatine insensitive 1-2* (*coi1-2*)—the JA receptor mutant—showed partially defective upregulation of *ERF109* from 10 min to 1 h (Fig. 2b). Analyses from the *ASA1_{pro}:GUS* (β -glucuronidase) reporter line (Fig. 2c–e) and qRT-PCR (Fig. 2h) showed that *ASA1* was gradually

¹National Key Laboratory of Plant Molecular Genetics, CAS Center for Excellence in Molecular Plant Sciences, Shanghai Institute of Plant Physiology and Ecology, Chinese Academy of Sciences, Shanghai, China. ²University of Chinese Academy of Sciences, Beijing, China. ³School of Life Sciences, Nantong University, Nantong, China. ⁴School of Public Health, Nantong University, Nantong, China. ⁵Shanghai-Hong Kong Joint Laboratory in Chemical Synthesis, Shanghai Institute of Organic Chemistry, Chinese Academy of Sciences, Shanghai, China. ⁶Department of Plant Pathology, University of Georgia, Athens, GA, USA. ⁷Department of Neurosurgery, Stanford University School of Medicine, Stanford, CA, USA. ⁸Department of Psychiatry and Behavioral Sciences, Stanford University School of Medicine, Stanford, CA, USA. ⁹These authors contributed equally: Guifang Zhang, Fei Zhao, Lyuqin Chen. *e-mail: xulin01@sibs.ac.cn

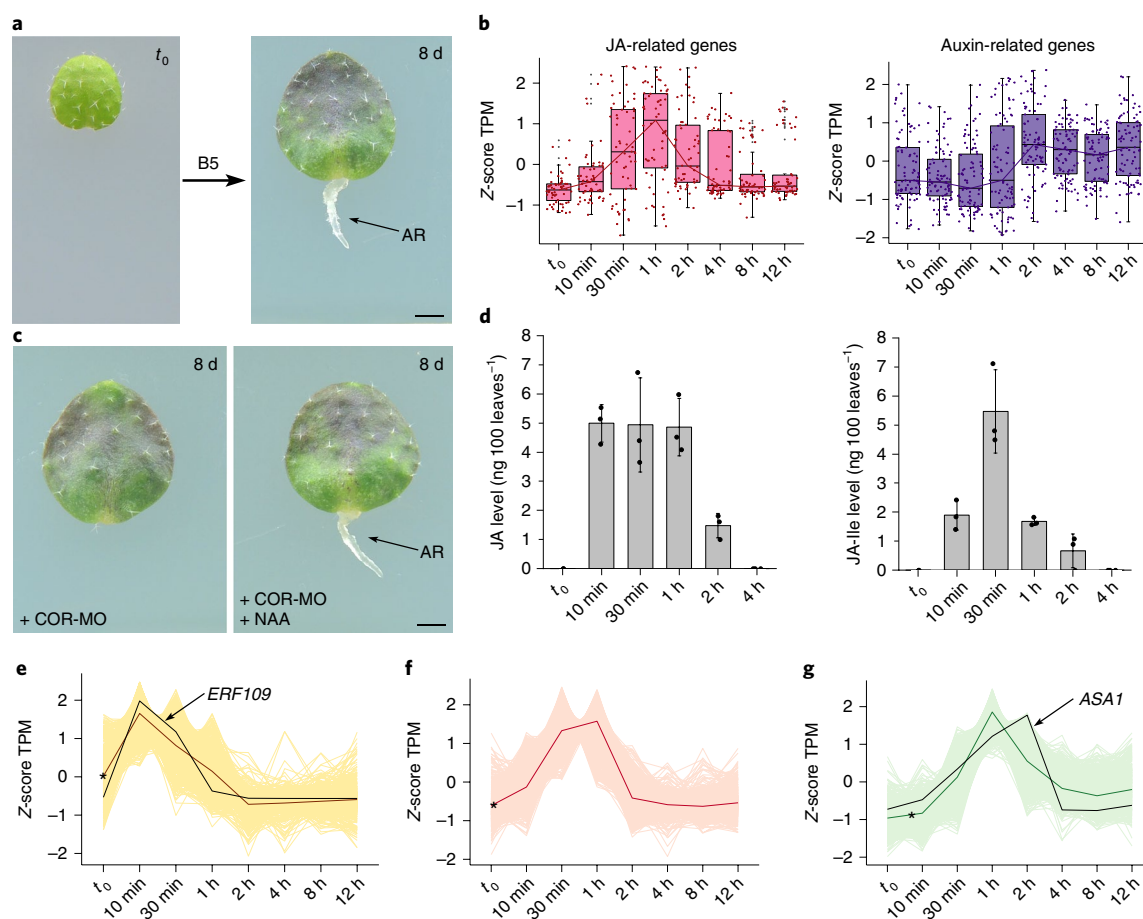


Fig. 1 | JA serves as a wound signal to promote DNRR. **a**, Wild-type Col-0 leaf explants cultured on B5 medium without exogenous hormones under 24 h light conditions. Approximately 67% of cuttings (20/30) had formed adventitious roots (AR) at 8 d. **b**, Box plots showing RNA-seq analysis of JA- (left) and auxin-related genes (right) in response to wounding after detachment of Col-0 leaves. JA- ($n = 60$) and auxin-related genes ($n = 89$) were selected based on the gene annotations related to JA and auxin pathways and the average of TPM > 1 in the RNA-seq data. In each box plot, the horizontal bar in the box indicates the median value. The upper and lower hinges of each box indicate the 75 and 25% ranges of the reported values, respectively. The whiskers correspond to $1.5 \times$ the interquartile range. Black points indicate outliers. Pink points (JA-related genes) or purple points (auxin-related genes) indicate gene values. JA- and auxin-related genes are listed in Supplementary Table 1. **c**, Only ~3% of Col-0 leaf explants (1/30) had formed ARs at 8 d on B5 medium with $50 \mu\text{M}$ COR-MO treatment (left). This rooting defect was partially rescued by $0.1 \mu\text{M}$ NAA treatment, with around ~37% of leaf explants (11/30) forming roots by 8 d (right). For the control, see **a**. **d**, Free JA (left) and JA-Ile (right) levels in leaf explants from t_0 to 4 h after leaf detachment. Error bars show s.d. from two or three biological repeats ($n > 140$ leaf explants per biological repeat). Individual values (black dots) and means (bars) are shown. **e–g**, RNA-seq data showing cluster-1 (**e**; $n = 558$ genes), -2 (**f**; $n = 1,120$ genes) and -3 (**g**; $n = 982$ genes) genes upregulated in response to wounding after the detachment of Col-0 leaves (see Supplementary Table 1). The *ERF109*-*ASA1* module was selected for further analysis of its role in regeneration. Asterisks indicate average values. Scale bars, 1 mm in **a** and **c**.

upregulated primarily in the vasculature from 30 min, had peak transcript levels at 2 h and was then downregulated at 4 h. Mutations in the *ERF109*-binding *cis* element¹⁰ on the *ASA1* promoter (*mASA1_{pro}:GUS*) (Fig. 2c–g) or mutations in the *COI1* or *ERF109* gene (Fig. 2h) resulted in the loss of *ASA1* upregulation at 2 h. Phenotypic analyses revealed that the *coi1-2*, *erf109-1* and *asa1-2* mutants showed defective rooting from leaf explants (Fig. 2i). The auxin level in wild-type leaf explants was elevated at 12 h, and this elevation was defective in the leaf explants of *coi1-2* and *erf109-1* (Supplementary Fig. 3). Treatment with ANT rescued the rooting defect in the *coi1-2*, *erf109-1* or *asa1-2* mutant backgrounds (Fig. 2i). In addition, overexpression of *ASA1* (*35S_{pro}:ASA1*) also rescued the rooting defect in *coi1-2* leaf explants (Fig. 2i). Taken together, these data suggest that the JA-*ERF109*-*ASA1* pathway may serve as a wound signalling pathway to promote auxin biosynthesis for DNRR from leaf explants.

Next, we tested the molecular mechanism by which *ERF109* quickly activates *ASA1*. The results of another study indicated that *SET DOMAIN GROUP8* (*SDG8*)-mediated histone H3 lysine 36 trimethylation (H3K36me3) might function in the JA-mediated plant defence response to pathogens¹⁹. Therefore, we tested whether *SDG8*-mediated H3K36me3 functions in the JA-*ERF109*-*ASA1* wound signalling pathway. The result showed that upregulation of *ERF109* at 10 min was not affected in *sdg8-2* leaf explants (Fig. 3a), but upregulation of *ASA1* at 2 h was significantly defective (Fig. 3b,g). Phenotypic analyses revealed that the *sdg8-2* mutant leaf explants showed defective rooting (Fig. 3c). This defect was partially rescued by ANT treatment or *ASA1* overexpression (Fig. 3c). Furthermore, overexpression of *ERF109*-*GLUCOCORTICOID RECEPTOR* (*35S_{pro}:ERF109-GR*) resulted in upregulation of *ASA1* in leaves, but this upregulation was partially defective in the *sdg8-2* background (Fig. 3d). We then tested the H3K36me3 levels in

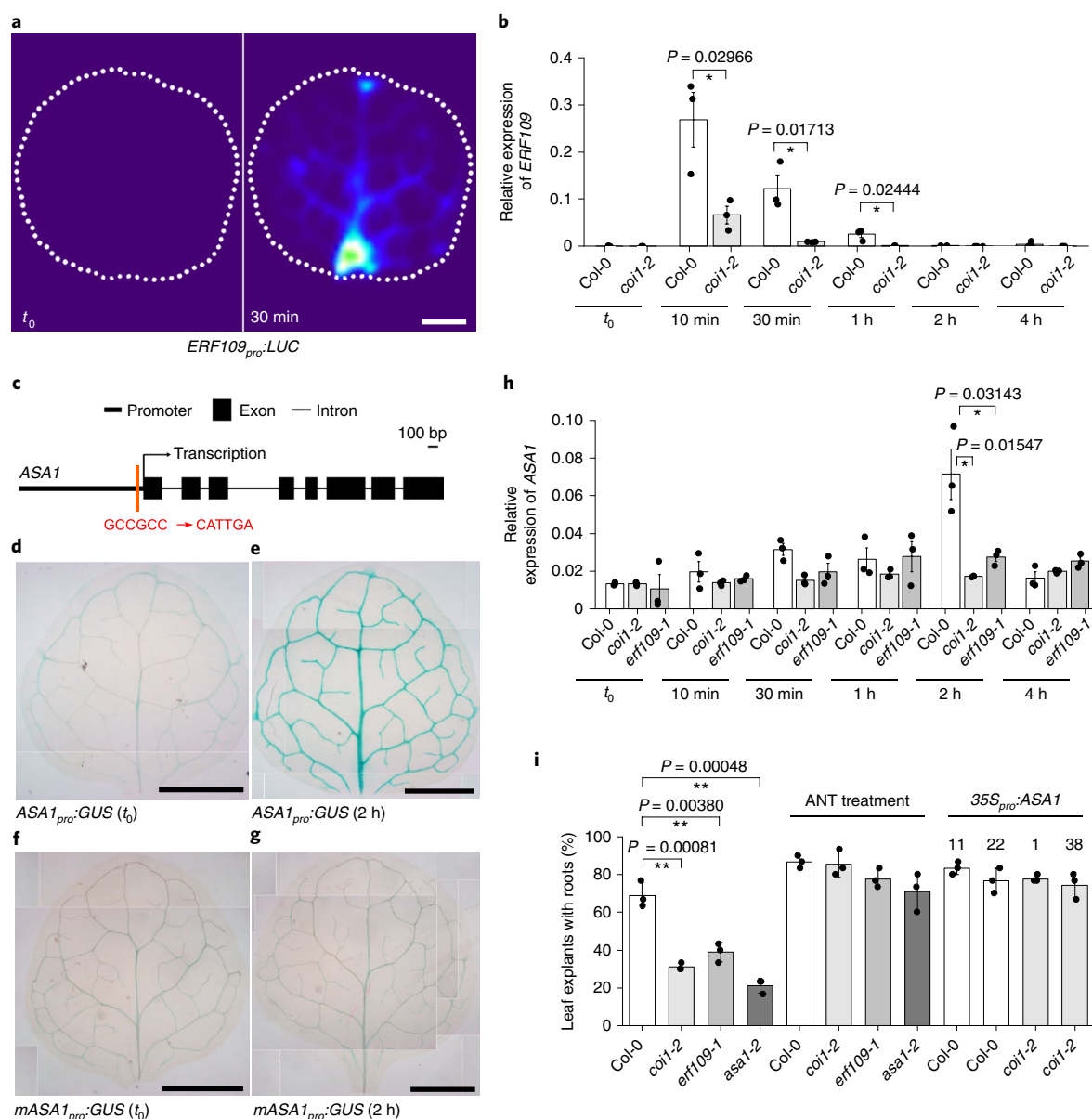


Fig. 2 | JA-ERF109-ASA1 wound signalling pathway in DNRR. a, Analysis of *ERF109_{pro}::LUC* leaf explants at t_0 (left) and 30 min (right). Two independent lines were analysed and showed similar results. **b**, qRT-PCR analysis of *ERF109* transcript levels in Col-0 and *coi1-2* leaf explants from t_0 to 4 h. **c**, Schematic of the *ASA1* gene showing the mutated ERF109-binding element (GCCGCC to CATTGA) on the promoter (red line). **d-g**, GUS staining of *ASA1_{pro}::GUS* (d and e) and *mASA1_{pro}::GUS* (f and g) leaf explants at t_0 (d and f) and 2 h (e and g). The images are composites of smaller images of the same leaf explant because the entire leaf explant did not fit within a single visual field of the microscope. Two independent lines from each transgenic experiment were analysed and showed similar results. **h**, qRT-PCR analysis of *ASA1* transcript levels in Col-0, *coi1-2* and *erf109-1* leaf explants from t_0 to 4 h. **i**, Percentages of Col-0, *coi1-2*, *erf109-1* and *asa1-2* leaf explants that regenerated ARs by 8 d on B5 medium. The addition of 5 μ M ANT rescued rooting defects in each mutant. $35S_{pro}::ASA1$ also rescued the rooting defect in *coi1-2*. Independent $35S_{pro}::ASA1$ lines in the Col-0 (lines 11 and 22) or *coi1-2* background (lines 1 and 38) were tested and showed similar results. Error bars show s.d. (i) or s.e.m. (b and h) from three biological repeats. * $P < 0.05$ and ** $P < 0.01$ in two-tailed Student's *t*-tests compared with each Col-0 control (b, h and i). Each biological replicate was performed with three technical replicates for qRT-PCR (b and h). $n = 30$ leaf explants in each biological repeat for phenotype analysis (i). Individual values (black dots) and means (bars) are shown (b, h and i). Scale bars, 1 mm in a and d-g.

t_0 leaf explants from wild-type and *sdg8-2* plants by ChIP assay. In wild-type leaves, the H3K36me3 levels were highly enriched on the *ASA1* locus at t_0 (Fig. 3e-g), suggesting that H3K36me3 is deposited before wounding. The H3K36me3 levels on the *ASA1* locus at t_0 were significantly lower in *sdg8-2* leaves than in Col-0 leaves (Fig. 3e-g). Taken together, these data indicate that quick upregulation of *ASA1* by ERF109 within 2 h is dependent on the presence of SDG8-mediated H3K36me3 on the *ASA1* locus. H3K36me3 seems to be an 'on-call'

mechanism that is deposited on the *ASA1* locus before wounding and facilitates the upregulation of *ASA1* by ERF109 after wounding.

We further analysed whether SDG8-mediated H3K36me3 is generally involved in JA-mediated gene upregulation in response to wounding by analysing the ChIP-seq data of genome-wide H3K36me3 (ref. 20) and the RNA-seq data of changes in the transcriptome in Col-0, *sdg8-2* and *coi1-2* leaf explants (2 h versus t_0) (Supplementary Fig. 4). The result suggested that rapid

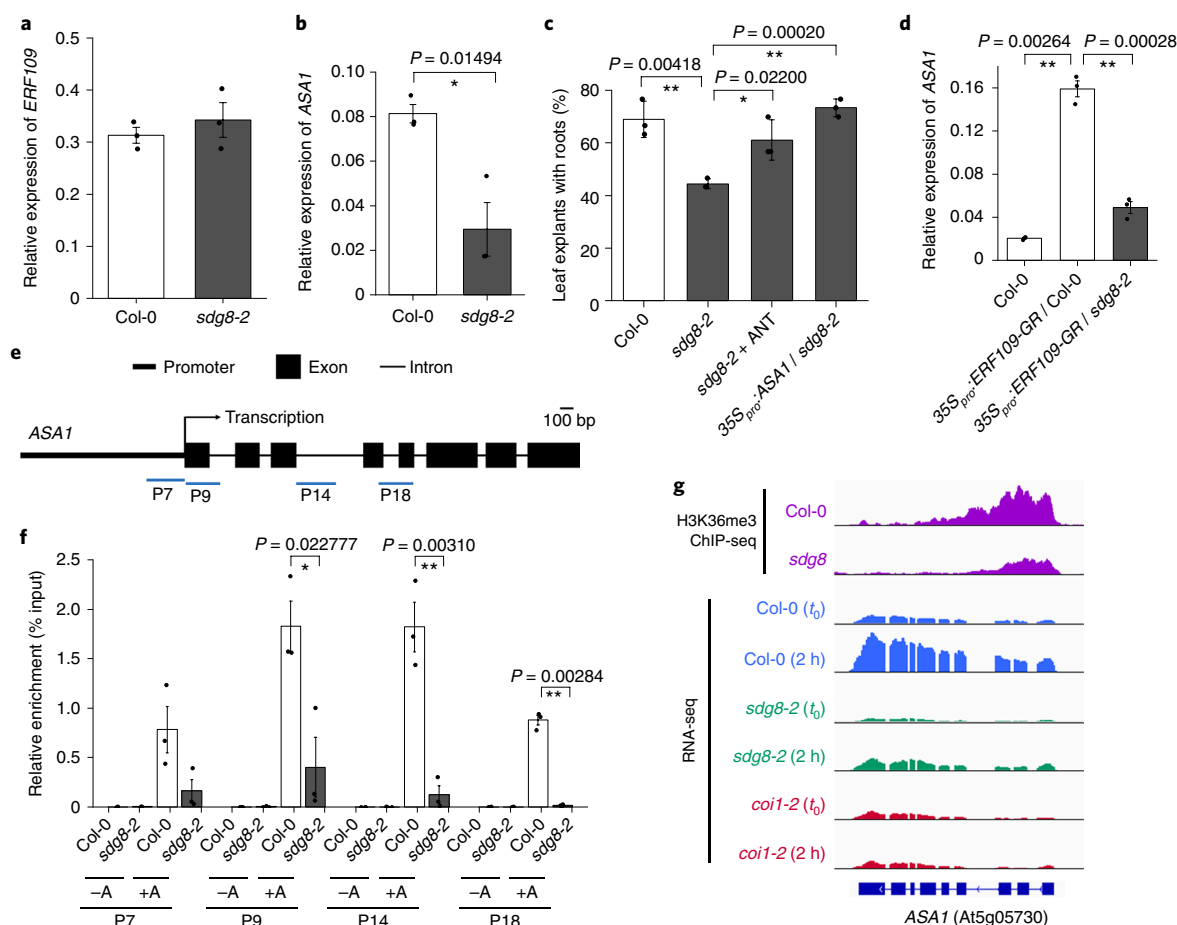


Fig. 3 | SDG8-mediated H3K36me3 is involved in wound response. **a,b**, qRT-PCR analysis of transcript levels of *ERF109* (**a**) or *ASA1* (**b**) in Col-0 and *sdg8-2* at 10 min (**a**) or 2 h (**b**) after leaf detachment. **c**, Percentages of Col-0, *sdg8-2* and *35S_{pro}:ASA1* (line 11)/*sdg8-2* leaf explants that regenerated ARs by 8 d on B5 medium. The rooting defect in *sdg8-2* could be partially rescued by 5 μ M ANT treatment. **d**, qRT-PCR analysis of *ASA1* transcript levels in Col-0, *35S_{pro}:ERF109-GR* and *35S_{pro}:ERF109-GR/sdg8-2* leaves at *t*₀. The 12-d-old seedlings on $\frac{1}{2}$ MS medium were first treated with 10 μ M CHX for 30 min, then with 15 μ M dexamethasone for 4 h. Leaves were used for RNA extraction. **e**, Schematic of the *ASA1* gene showing PCR fragments in ChIP analysis (blue lines below the gene). **f**, ChIP analysis of H3K36me3 levels in *t*₀ leaf explants from Col-0 and *sdg8-2*. The results were normalized against those produced by input, which had an arbitrarily fixed value of 1.0. Anti-H3K36me3 antibody was used (+A). No antibody served as negative control (–A). **g**, Integrative Genomics Viewer screen shots showing H3K36me3 levels²⁰ (Col-0 and *sdg8*) at the *ASA1* locus, and expression levels of *ASA1* in Col-0, *sdg8-2* and *coi1-2* (*t*₀ and 2 h). Two independent RNA-seq experiments were performed and showed similar results. Error bars show s.e.m. (**a,b,d** and **f**) or s.d. (**c**) from three biological repeats. **P* < 0.05 and ***P* < 0.01 in two-tailed Student's *t*-tests (**b–d** and **f**). Each biological replicate was performed with three technical replicates for qRT-PCR (**a,b** and **d**) and ChIP (**f**) analyses. *n* = 30 leaf explants in each biological repeat for phenotype analysis (**c**). Individual values (black dots) and means (bars) are shown (**a–d** and **f**).

upregulation of a group of genes (cluster-10 genes; Supplementary Fig. 4 and Supplementary Table 1) by the JA-mediated wound signalling pathway within 2 h could be dependent on pre-deposition of SDG8-mediated H3K36me3. However, the mechanism by which SDG8-mediated H3K36me3 promotes JA-mediated gene upregulation remains elusive.

Since the JA-mediated wound signalling pathway predominantly functions within 2 h of leaf detachment, we explored the mechanism by which wound signalling was shut down at 4 h. Using the *ERF109_{pro}:ERF109-GUS* marker line, we found that the ERF109-GUS fused protein was present from 30 min to 4 h after leaf detachment (Fig. 4a); however, *ERF109-GUS* transcripts were not detected at 4 h (Fig. 4b). The ERF109 protein was unable to upregulate *ASA1* at 4 h because the *ASA1* transcriptional level in wild-type leaf explants at 4 h after wounding decreased to a level comparable to that at *t*₀ (Fig. 2h). This suggested that there was some mechanism that inhibited the protein function of ERF109 at 4 h. We noticed that JA was not detected at 4 h in wild-type leaf explants (Fig. 1d),

indicating that JASMONATE-ZIM-DOMAIN (JAZ) proteins, which are degraded in the presence of JA^{21,22}, might function at 4 h. Analysis of *ERF109_{pro}:ERF109-Venus* and *JAZ9_{pro}:JAZ9-Venus* marker lines confirmed that the ERF109-Venus and JAZ9-Venus proteins are both present in leaf explants at 4 h (Supplementary Fig. 5). JAZ proteins are known to inhibit the activity of transcription factors by direct protein interaction²³. The results of co-immunoprecipitation (Co-IP) and yeast two-hybrid assays showed that many JAZ proteins (for example, JAZ5, 8 and 9) could interact with ERF109 (Fig. 4c,d). Coexpression of *35S_{pro}:ERF109-MYC-cYFP* (C-terminal fragment of yellow fluorescent protein) together with *ASA1_{pro}:LUC* could activate the LUC response in tobacco leaves, while this activation of the LUC response was partially inhibited by *35S_{pro}:JAZ9-HA-nYFP* (N-terminal fragment of YFP), indicating that JAZ9 might inhibit ERF109 activity in planta (Fig. 4e). In addition, we cultured wild-type leaf explants on B5 medium for 2 h to allow *ASA1* upregulation by ERF109, then on B5 medium with cycloheximide (CHX; a protein synthesis inhibitor) or B5 medium

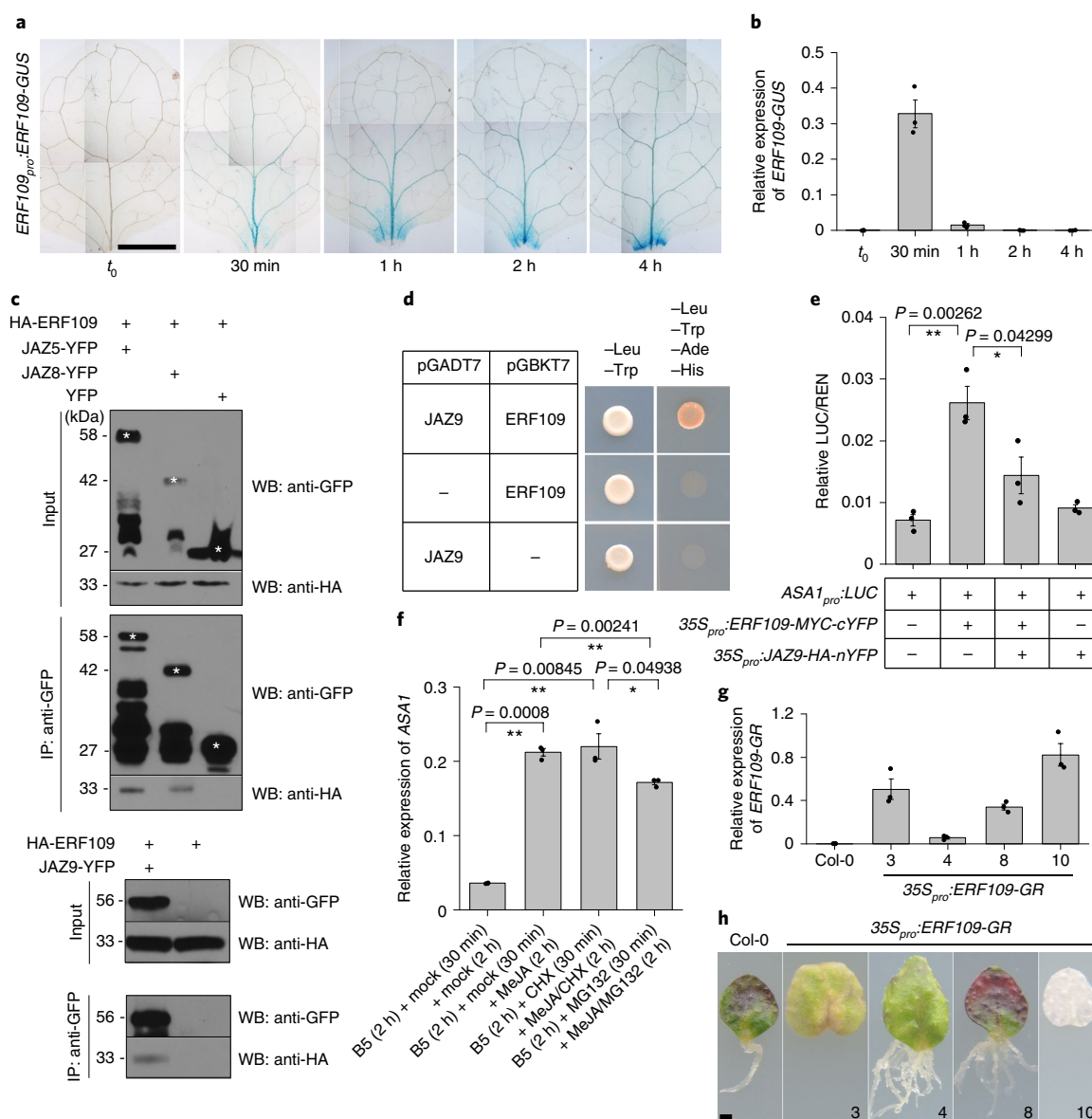


Fig. 4 | Prevention of hypersensitivity to JA-mediated wound signalling. **a**, GUS staining of *ERF109_{pro}:ERF109-GUS* from t_0 to 4 h after leaf detachment. Images are composites of smaller images of the same leaf explant because the entire leaf explant did not fit within a single visual field of the microscope. Two independent lines were analysed and showed similar results. **b**, qRT-PCR analysis of transcript levels of *ERF109-GUS* in *ERF109_{pro}:ERF109-GUS* leaf explants from t_0 to 4 h. **c**, Co-IP analysis of the interaction between ERF109 and JAZ5/8/9 in tobacco leaves using *35S_{pro}:HA-ERF109*, *35S_{pro}:JAZ5-YFP*, *35S_{pro}:JAZ8-YFP* and *35S_{pro}:JAZ9-YFP*. White asterisks indicate YFP or YFP-fused proteins. Two biological repeats were performed and showed similar results. IP, immunoprecipitation; WB, Western blot. **d**, Yeast two-hybrid analysis of the interaction between ERF109 and JAZ9. Two biological repeats were performed and showed similar results. **e**, Relative ratio of firefly LUC to Renilla luciferase (REN) activity in tobacco leaves cotransformed with *ASA1_{pro}:LUC* and *35S_{pro}:ERF109-MYC-cYFP* with or without *35S_{pro}:JAZ9-HA-nYFP*. Sole transformation with *ASA1_{pro}:LUC* or cotransformation with *ASA1_{pro}:LUC* and *35S_{pro}:JAZ9-HA-nYFP* served as negative controls. **f**, qRT-PCR analysis of *ASA1*. Wild-type leaf explants were first cultured on B5 medium for 2 h, transferred to B5 medium containing 10 μ M CHX or 50 μ M MG132 for 30 min, and then transferred to B5 medium containing 10 μ M methyl jasmonate (MeJA) together with 10 μ M CHX or 50 μ M MG132 for 2 h. B5 medium containing ethanol and dimethyl sulfoxide (mock) served as a negative control. Sole MeJA treatment served as positive control. **g**, qRT-PCR analysis of *ERF109* transcript levels in leaves from Col-0 and *35S_{pro}:ERF109-GR* lines (numbers 3, 4, 8 and 10) at t_0 . **h**, Phenotypic analysis of rooting from Col-0 and *35S_{pro}:ERF109-GR* leaf explants at 14 d of culture on B5 medium containing 10 μ M dexamethasone. More than 20 leaves were analysed for each line (numbers 3, 4, 8 and 10) and showed the same results. Error bars (**b**, **e**, **f** and **g**) show s.e.m. from three biological repeats. Each biological replicate was analysed with three (**b**, **f** and **g**) or five (**e**) technical replicates. * $P < 0.05$ and ** $P < 0.01$ in two-tailed Student's *t*-tests (**e** and **f**). Scale bars, 1 mm in **a** and **h**. Individual values (black dots) and means (bars) are shown (**b** and **e**–**g**).

with MG132 (a protein degradation inhibitor) for 30 min pre-incubation, and finally on B5 medium with JA/CHX for JAZ degradation but no further JA-induced protein production, or B5 medium with JA/MG132 for the prevention of JAZ degradation by JA, for 2 h, respectively. The results showed that *ASA1* expression could

be kept at a higher level in the JA/CHX treatment than in the JA/MG132 treatment or the mock (Fig. 4f), indicating that the degradation of JAZ proteins can result in higher ERF109 activity for *ASA1* transcription. Based on these observations, we hypothesized that, at 4 h after leaf detachment, the loss of JA accumulation in leaf

explants leads to the interaction between JAZs and ERF109, and inhibition of ERF109 activity, resulting in the prevention of hypersensitivity to wound signalling. Furthermore, it is possible that *ERF109* peak expression at 10 min could also be regulated by other signals^{24–26} because *ERF109* was still slightly upregulated in *coi1-2* leaf explants after detachment (Fig. 2b), and adventitious rooting is not fully and strictly dependent on the *COI1* pathway (Fig. 2i). Therefore, JAZs probably also prevent hypersensitivity of leaves to ERF109 accumulation in response to those signals.

Finally, we tested whether the turning down of wound signalling after 2 h is required for DNRR. We obtained four lines of transgenic plants with inducible overexpression of *ERF109* (*35S_{pro}:ERF109-GR*): two lines (3 and 10) showed high *ERF109-GR* overexpression levels, and two (4 and 8) showed moderate *ERF109-GR* overexpression levels (Fig. 4g). Moderate overexpression of *ERF109* (lines 4 and 8) enhanced adventitious root regeneration from leaf explants; however, high *ERF109* overexpression (lines 3 and 10) resulted in defective rooting and senescence of leaf explants (Fig. 4h). These findings indicate that high-level and constant expression of ERF109 inhibits regeneration. In addition, constant JA treatment inhibited rooting from leaf explants (Supplementary Fig. 6), indicating that constant JA-mediated wound signalling is harmful for DNRR. This explains why some studies have observed that JA inhibits adventitious root formation²⁷.

Here, we summarize the events in wound signalling that lead to DNRR from leaf explants. Wounding seems to have at least two roles. First, it creates a physical barrier to arrest auxin flux, resulting in an auxin maximum at the wounded site⁶. Second, it enhances auxin biosynthesis to promote the efficiency of regeneration (see the model in Supplementary Fig. 7). Specifically, wounding induces JA production in leaf explants and activates *ERF109* expression, which in turn upregulates *ASA1* expression within 2 h of leaf detachment. Highly expressed *ASA1* enhances auxin biosynthesis, then promotes rooting from leaf explants. After 2 h, the JA level decreases, resulting in the interaction of JAZs with ERF109 to inhibit ERF109 activity to prevent hypersensitivity to wound signalling. In addition, pre-deposition of SDG8-mediated H3K36me3 is required for upregulation of expression of many genes by JA-mediated wound signalling within 2 h of wounding. Overall, our results indicate that JA-mediated wound signalling is dynamically controlled and cooperates with an epigenetic mechanism to promote DNRR from leaf explants.

Methods

Plant materials, culture conditions and hormone detection. *Arabidopsis* Col-0 was used as the wild-type. The *coi1-2*, *erf109-1*, *asa1-2* and *sdg8-2* mutants have been described previously^{9–11,28}. For construction of *35S_{pro}:ERF109-GR*, *35S_{pro}:eGFP-ERF109* and *35S_{pro}:ASA1*, we inserted the *ERF109* or *ASA1* complementary DNA (cDNA) into the pMON530-GR, pMON530-eGFP or pMON530 vector. *35S_{pro}:HA-ERF109* was constructed by inserting *HA-ERF109* into the pGWB614 vector. *35S_{pro}:JAZ5-YFP*, *35S_{pro}:JAZ8-YFP* and *35S_{pro}:JAZ9-YFP* have been described previously²⁹. *ERF109_{pro}:LUC* was constructed by inserting the 3.1-kilobase (kb) *ERF109* promoter, followed by the *LUC* coding region, into pBI101 to replace the *GUS* gene. *ASA1_{pro}:LUC* was constructed by inserting the 1.2-kb *ASA1* promoter into pGreenII-0800. *ASA1_{pro}:GUS* and *mASA1_{pro}:GUS* were constructed by inserting the *ASA1* promoter or the *ASA1* promoter with the mutated ERF109-binding element (GCCGCC to CATTGA)¹⁰, respectively, into pBI101. *ERF109_{pro}:ERF109-GUS* was constructed by inserting the 3-kb *ERF109* promoter followed by the *ERF109* genomic gene body into pBI101. *ERF109_{pro}:ERF109-Venus* or *JAZ9_{pro}:JAZ9-Venus* were constructed by inserting the 3-kb *ERF109* promoter and the *ERF109* genomic gene body, or the 1.5-kb *JAZ9* promoter and the *JAZ9* genomic gene body, followed by the *Venus* coding region, into pMY122 (modified from pBI101) to replace the *GUS* gene, respectively. *AD-ERF109* and *BD-JAZ9* were constructed by inserting *ERF109* and *JAZ9* cDNA into the pGADT7 and pGBKT7 vectors, respectively. *35S_{pro}:JAZ9-HA-nYFP* and *35S_{pro}:ERF109-MYC-cYFP* were constructed by inserting *JAZ9* and *ERF109* cDNA into the pMY304 and pMY305 vectors, respectively. Transgenic plants were obtained by *Agrobacterium tumefaciens*-mediated transformation.

For DNRR, *Arabidopsis* seeds were germinated on ½ MS medium at 22°C under a 16 h light/8 h dark photoperiod^{30,31}. Detached leaf explants from 12-day-old seedlings were cultured on B5 medium without sucrose at 22°C under 24 h

light conditions^{31,32}. Leaf explants from 14-day-old *ERF109_{pro}:LUC* seedlings were used for LUC observations. COR-MO was synthesized as described previously¹⁷. The dual LUC assay in tobacco leaves was performed using the Dual-Luciferase Reporter Assay System (Promega).

For JA detection, JA was extracted from leaf explants as previously reported³³. Samples were re-dissolved in 70% methanol for liquid chromatography mass spectrometry analysis using an Agilent 1200 system (Accurate-Mass Q-TOF), and the mass spectrometry analysis was performed in the negative-ion mode. Dihydrojasmonic acid was used as an internal standard, and JA, JA-Ile and dihydrojasmonic acid were detected at *m/z* 209.1180, 322.2000 and 211.1340, respectively.

For auxin detection, 30 leaf explants from each sample were ground by liquid nitrogen, dissolved by 100 µl phosphate buffered saline for 10 min on ice, and centrifuged at 12,000 r.p.m. at 4°C. The auxin concentration was tested with 10 µl supernatant for each technical repeat using electrochemical detection of auxin as previously described^{34,35}.

Co-IP, yeast two-hybrid, ChIP and qRT-PCR analyses. The Co-IP, yeast two-hybrid, ChIP and qRT-PCR analyses were performed as described previously^{29,36–38}. The qRT-PCR results represent relative expression levels, which were normalized against those produced using *ACTIN* primers, which had an arbitrarily fixed value of 1.0. ChIP and Co-IP analyses were performed using the anti-trimethyl-H3K36 antibody (ab9050; Abcam), anti-HA antibody (11867431001; Rohce), anti-GFP antibody (11814460001; Rohce) and HA isolation kit (130-091-122; MACS Miltenyi Biotec). The primers used for real-time PCR and molecular cloning are listed in Supplementary Table 2.

RNA-seq and ChIP-seq analyses. For RNA-seq analyses, RNA was extracted using TRIzol. Library construction and deep sequencing were carried out using the Illumina HiSeq 3000 platform following the manufacturer's instructions (Genenergy Biotechnology). Raw sequencing reads were quality trimmed using Trimmomatic³⁹, and the clean reads were mapped to the *Arabidopsis thaliana* genome (TAIR10) using Bowtie 1.2.2 (ref. 40) for DNA sequencing and STAR 2.5.4b⁴¹ for RNA sequencing. The returned alignments were stringently filtered to remove duplicates (only DNA sequencing), ambiguously mapped reads and read pairs with conflicting alignments.

For RNA-seq data analysis, RSEM version 1.2.31 (ref. 42) was used to quantify gene abundance and the transcript levels of individual genes, which are shown as the average of transcripts per million (TPM) from two biological replicates. All genes were filtered by the average of TPM > 1 at 8 time points to remove genes with low transcript levels. To compare time-series gene expression data, the final 7,835 filtered genes, which averaged TPM > 1, coefficient of variation > median coefficient of variation, and membership values (defined by Mfuzz package) > 0.5, were subjected to unsupervised clustering by the fuzzy c-means algorithm as implemented in the Mfuzz package⁴³. Differentially expressed genes were detected by EBSeq⁴⁴ based on the combined criteria: |log₂[fold change]| > 1 and false discovery rate < 0.05.

For ChIP-seq data analysis, MACS2 (ref. 45) with an additional parameter ‘-broad’ was used to identify read-enriched regions (peaks) in the H3K36me3 ChIP-seq data. Next, differential occupancy analysis (|log₂[fold change]| > 1 and false discovery rate < 0.05) was performed using the DiffBind⁴⁶ package. The H3K36me3 target gene was defined as the gene with given peak(s) in the gene body region. Integrative Genomics Viewer⁴⁷ was used for illustrating the genomic tracks, and we used reads per kilobase per million reads to normalize the number of reads per bin.

The ChIP-seq data used in this study were obtained from the National Center for Biotechnology Information Sequence Read Archive (<https://www.ncbi.nlm.nih.gov/sra>; accession number SRX746966)³⁰. The following datasets were used: WT-H3K36me3 and input (SRR1635352, SRR1635390, SRR1635829 and SRR1635841); and *sdg8*-H3K36me3 and input (SRR1635391, SRR1635488, SRR1635842 and SRR1635844). The RNA-seq data have been deposited in the Gene Expression Omnibus (<http://www.ncbi.nlm.nih.gov/geo/>) and assigned the identifier accession GSE120418.

Reporting Summary. Further information on research design is available in the Nature Research Reporting Summary linked to this article.

Data availability

The data that support the findings of this study are available from the corresponding author upon request.

Received: 14 September 2018; Accepted: 15 March 2019;
Published online: 22 April 2019

References

- Chen, L., Sun, B., Xu, L. & Liu, W. Wound signaling: the missing link in plant regeneration. *Plant Signal. Behav.* **11**, e1238548 (2016).
- Ikeuchi, M. et al. Wounding triggers callus formation via dynamic hormonal and transcriptional changes. *Plant Physiol.* **175**, 1158–1174 (2017).

3. Birnbaum, K. D. & Sanchez Alvarado, A. Slicing across kingdoms: regeneration in plants and animals. *Cell* **132**, 697–710 (2008).
4. Xu, L. & Huang, H. Genetic and epigenetic controls of plant regeneration. *Curr. Top. Dev. Biol.* **108**, 1–33 (2014).
5. Liu, J. et al. *WOX11* and *12* are involved in the first-step cell fate transition during de novo root organogenesis in *Arabidopsis*. *Plant Cell* **26**, 1081–1093 (2014).
6. Xu, L. De novo root regeneration from leaf explants: wounding, auxin, and cell fate transition. *Curr. Opin. Plant Biol.* **41**, 39–45 (2018).
7. Chen, L. et al. *YUCCA*-mediated auxin biogenesis is required for cell fate transition occurring during de novo root organogenesis in *Arabidopsis*. *J. Exp. Bot.* **67**, 4273–4284 (2016).
8. Niyogi, K. K. & Fink, G. R. Two anthranilate synthase genes in *Arabidopsis*: defense-related regulation of the tryptophan pathway. *Plant Cell* **4**, 721–733 (1992).
9. Sun, J. et al. *Arabidopsis* *ASA1* is important for jasmonate-mediated regulation of auxin biosynthesis and transport during lateral root formation. *Plant Cell* **21**, 1495–1511 (2009).
10. Cai, X. T. et al. *Arabidopsis* *ERF109* mediates cross-talk between jasmonic acid and auxin biosynthesis during lateral root formation. *Nat. Commun.* **5**, 5833 (2014).
11. Zhao, Z., Yu, Y., Meyer, D., Wu, C. & Shen, W. H. Prevention of early flowering by expression of *FLOWERING LOCUS C* requires methylation of histone H3 K36. *Nat. Cell Biol.* **7**, 1256–1260 (2005).
12. Da Costa, C. T. et al. When stress and development go hand in hand: main hormonal controls of adventitious rooting in cuttings. *Front. Plant Sci.* **4**, 133 (2013).
13. Druege, U., Franken, P. & Hajirezaei, M. R. Plant hormone homeostasis, signaling, and function during adventitious root formation in cuttings. *Front. Plant Sci.* **7**, 381 (2016).
14. Ahkami, A. H. et al. Molecular physiology of adventitious root formation in *Petunia hybrida* cuttings: involvement of wound response and primary metabolism. *New Phytol.* **181**, 613–625 (2009).
15. Fattorini, L. et al. Adventitious rooting is enhanced by methyl jasmonate in tobacco thin cell layers. *Planta* **231**, 155–168 (2009).
16. Lischweski, S., Muchow, A., Guthorl, D. & Hause, B. Jasmonates act positively in adventitious root formation in petunia cuttings. *BMC Plant Biol.* **15**, 229 (2015).
17. Monte, I. et al. Rational design of a ligand-based antagonist of jasmonate perception. *Nat. Chem. Biol.* **10**, 671–676 (2014).
18. Wang, Z. et al. Identification and characterization of COI1-dependent transcription factor genes involved in JA-mediated response to wounding in *Arabidopsis* plants. *Plant Cell Rep.* **27**, 125–135 (2008).
19. Berr, A. et al. *Arabidopsis* histone methyltransferase SET DOMAIN GROUP8 mediates induction of the jasmonate/ethylene pathway genes in plant defense response to necrotrophic fungi. *Plant Physiol.* **154**, 1403–1414 (2010).
20. Li, Y. et al. The histone methyltransferase SDG8 mediates the epigenetic modification of light and carbon responsive genes in plants. *Genome Biol.* **16**, 79 (2015).
21. Thines, B. et al. JAZ repressor proteins are targets of the SCF(COI1) complex during jasmonate signalling. *Nature* **448**, 661–665 (2007).
22. Chini, A. et al. The JAZ family of repressors is the missing link in jasmonate signalling. *Nature* **448**, 666–671 (2007).
23. Kazan, K. & Manners, J. M. JAZ repressors and the orchestration of phytohormone crosstalk. *Trends Plant Sci.* **17**, 22–31 (2012).
24. Bahieldin, A. et al. Multifunctional activities of ERF109 as affected by salt stress in *Arabidopsis*. *Sci. Rep.* **8**, 6403 (2018).
25. Bahieldin, A. et al. Ethylene responsive transcription factor ERF109 retards PCD and improves salt tolerance in plant. *BMC Plant Biol.* **16**, 216 (2016).
26. Kong, X. et al. PHB3 maintains root stem cell niche identity through ROS-responsive AP2/ERF transcription factors in *Arabidopsis*. *Cell Rep.* **22**, 1350–1363 (2018).
27. Gutierrez, L. et al. Auxin controls *Arabidopsis* adventitious root initiation by regulating jasmonic acid homeostasis. *Plant Cell* **24**, 2515–2527 (2012).
28. Xu, L. et al. The SCF^{COI1} ubiquitin-ligase complexes are required for jasmonate response in *Arabidopsis*. *Plant Cell* **14**, 1919–1935 (2002).
29. Yang, L. et al. *Pseudomonas syringae* type III effector HopBB1 promotes host transcriptional repressor degradation to regulate phytohormone responses and virulence. *Cell Host Microb.* **21**, 156–168 (2017).
30. Murashige, T. & Skoog, F. A revised medium for rapid growth and bioassays with tobacco tissue culture. *Physiol. Plant.* **80**, 662–668 (1962).
31. Chen, X. et al. A simple method suitable to study de novo root organogenesis. *Front. Plant Sci.* **5**, 208 (2014).
32. Gamborg, O. L., Miller, R. A. & Ojima, K. Nutrient requirements of suspension cultures of soybean root cells. *Exp. Cell Res.* **50**, 151–158 (1968).
33. Mao, Y. B. et al. Jasmonate response decay and defense metabolite accumulation contributes to age-regulated dynamics of plant insect resistance. *Nat. Commun.* **8**, 13925 (2017).
34. Sun, L.-J. et al. Electrochemical mapping of indole-3-acetic acid and salicylic acid in whole pea seedlings under normal conditions and salinity. *Sens. Actuators B Chem.* **276**, 543–551 (2018).
35. Sun, L.-J. et al. Paper-based analytical devices for direct electrochemical detection of free IAA and SA in plant samples with the weight of several milligrams. *Sens. Actuators B Chem.* **247**, 336–342 (2017).
36. He, C., Chen, X., Huang, H. & Xu, L. Reprogramming of H3K27me3 is critical for acquisition of pluripotency from cultured *Arabidopsis* tissues. *PLoS Genet.* **8**, e1002911 (2012).
37. Li, G. et al. ISWI chromatin remodeling factors and their interacting RINGLET proteins act together in controlling the plant vegetative phase in *Arabidopsis*. *Plant J.* **72**, 261–270 (2012).
38. Xu, L. et al. Di- and tri- but not monomethylation on histone H3 lysine 36 marks active transcription of genes involved in flowering time regulation and other processes in *Arabidopsis thaliana*. *Mol. Cell Biol.* **28**, 1348–1360 (2008).
39. Bolger, A. M., Lohse, M. & Usadel, B. Trimmomatic: a flexible trimmer for Illumina sequence data. *Bioinformatics* **30**, 2114–2120 (2014).
40. Langmead, B., Trapnell, C., Pop, M. & Salzberg, S. L. Ultrafast and memory-efficient alignment of short DNA sequences to the human genome. *Genome Biol.* **10**, R25 (2009).
41. Dobin, A. et al. STAR: ultrafast universal RNA-Seq aligner. *Bioinformatics* **29**, 15–21 (2013).
42. Li, B. & Dewey, C. N. RSEM: accurate transcript quantification from RNA-Seq data with or without a reference genome. *BMC Bioinformatics* **12**, 323 (2011).
43. Kumar, L. & M, E. F. Mfuzz: a software package for soft clustering of microarray data. *Bioinformatics* **2**, 5–7 (2007).
44. Leng, N. et al. EBSeq: an empirical Bayes hierarchical model for inference in RNA-Seq experiments. *Bioinformatics* **29**, 1035–1043 (2013).
45. Zhang, Y. et al. Model-based analysis of ChIP-Seq (MACS). *Genome Biol.* **9**, R137 (2008).
46. Stark, R. & Brown, G. *DiffBind: differential binding analysis of ChIP-Seq peak data* (Cancer Research UK, 2018).
47. Thorvaldsdottir, H., Robinson, J. T. & Mesirov, J. P. Integrative Genomics Viewer (IGV): high-performance genomics data visualization and exploration. *Brief. Bioinform.* **14**, 178–192 (2013).

Acknowledgements

We thank the ABRC, Z. Zhu, G. A. Howe and D. Xie for providing the *Arabidopsis* seeds, Z. Zhu and W. Zhou for helpful discussion, Y. Liu from the Core Facility Centre of SIPPE for technical assistance on JA detection, and J. Pan and D. Cai for help on auxin concentration analysis. This work was supported by grants from the National Natural Science Foundation of China (31630007, 31770399 and 21375066), Strategic Priority Research Program of CAS (grant number XDB27030103), Key Research Program of CAS (QYZDB-SSW-SMC010), Youth Innovation Promotion Association of CAS (2014241 and 2014230) and National Key Laboratory of Plant Molecular Genetics.

Author contributions

G.Z., L.C. and L.X. designed the research. G.Z., F.Z. and Y.Z. performed the RNA-seq and ChIP-seq analyses. G.Z., Y.P., L.S. and N.B. analysed the auxin concentration. C.-X.C. and Z.Q. synthesized the COR-MO. L.Y. performed the Co-IP. G.Z., L.C. and T.Z. performed the other experiments. G.Z., F.Z., L.Y. and L.X. analysed the data. L.X. wrote the article.

Competing interests

The authors declare no competing interests.

Additional information

Supplementary information is available for this paper at <https://doi.org/10.1038/s41477-019-0408-x>.

Reprints and permissions information is available at www.nature.com/reprints.

Correspondence and requests for materials should be addressed to L.X.

Journal peer review information: *Nature Plants* thanks Jian Xu and the other anonymous reviewers for their contribution to the peer review of this work.

Publisher's note: Springer Nature remains neutral with regard to jurisdictional claims in published maps and institutional affiliations.

© The Author(s), under exclusive licence to Springer Nature Limited 2019

Reporting Summary

Nature Research wishes to improve the reproducibility of the work that we publish. This form provides structure for consistency and transparency in reporting. For further information on Nature Research policies, see [Authors & Referees](#) and the [Editorial Policy Checklist](#).

Statistical parameters

When statistical analyses are reported, confirm that the following items are present in the relevant location (e.g. figure legend, table legend, main text, or Methods section).

n/a Confirmed

- ☐ ☒ The exact sample size (n) for each experimental group/condition, given as a discrete number and unit of measurement
- ☐ ☒ An indication of whether measurements were taken from distinct samples or whether the same sample was measured repeatedly
- ☐ ☒ The statistical test(s) used AND whether they are one- or two-sided
Only common tests should be described solely by name; describe more complex techniques in the Methods section.
- ☒ ☐ A description of all covariates tested
- ☒ ☐ A description of any assumptions or corrections, such as tests of normality and adjustment for multiple comparisons
- ☐ ☒ A full description of the statistics including central tendency (e.g. means) or other basic estimates (e.g. regression coefficient) AND variation (e.g. standard deviation) or associated estimates of uncertainty (e.g. confidence intervals)
- ☒ ☐ For null hypothesis testing, the test statistic (e.g. F , t , r) with confidence intervals, effect sizes, degrees of freedom and P value noted
Give P values as exact values whenever suitable.
- ☒ ☐ For Bayesian analysis, information on the choice of priors and Markov chain Monte Carlo settings
- ☒ ☐ For hierarchical and complex designs, identification of the appropriate level for tests and full reporting of outcomes
- ☒ ☐ Estimates of effect sizes (e.g. Cohen's d , Pearson's r), indicating how they were calculated
- ☐ ☒ Clearly defined error bars
State explicitly what error bars represent (e.g. SD, SE, CI)

Our web collection on [statistics for biologists](#) may be useful.

Software and code

Policy information about [availability of computer code](#)

Data collection

Trimmomatic, TAIR10, Bowtie 1.2.2, STAR_2.5.4b

Data analysis

RSEM v1.2.31, Mfuzz package, EBSeq, MACS2, DiffBind package, Integrative Genomics Viewer (IGV)

For manuscripts utilizing custom algorithms or software that are central to the research but not yet described in published literature, software must be made available to editors/reviewers upon request. We strongly encourage code deposition in a community repository (e.g. GitHub). See the Nature Research [guidelines for submitting code & software](#) for further information.

Data

Policy information about [availability of data](#)

All manuscripts must include a [data availability statement](#). This statement should provide the following information, where applicable:

- Accession codes, unique identifiers, or web links for publicly available datasets
- A list of figures that have associated raw data
- A description of any restrictions on data availability

The ChIP-Seq data used in this study were obtained from the National Center for Biotechnology Information (NCBI) Sequence Read Archive (SRA, <https://www.ncbi.nlm.nih.gov/sra>; accession number SRX746966). The RNA-seq data from this article have been deposited in the Gene Expression Omnibus database (www.ncbi.nlm.nih.gov/geo) and assigned the identifier accession GSE120418.

Field-specific reporting

Please select the best fit for your research. If you are not sure, read the appropriate sections before making your selection.

☒ Life sciences ☐ Behavioural & social sciences ☐ Ecological, evolutionary & environmental sciences

For a reference copy of the document with all sections, see [nature.com/authors/policies/ReportingSummary-flat.pdf](https://www.nature.com/authors/policies/ReportingSummary-flat.pdf)

Life sciences study design

All studies must disclose on these points even when the disclosure is negative.

Sample size	We chose the sample size according to previous studies (Chen, et al. Front. Plant Sci. 5:208, 2014)
Data exclusions	No data was excluded from the analysis.
Replication	Each experiment was performed with at least two repeats.
Randomization	We did not apply randomization. Most of the experimental findings were related to comparative analysis between wild-type and transgenic or mutant lines
Blinding	Blinding was not relevant to this study, because there was no individual /subjective bias in experimentation or data analysis.

Reporting for specific materials, systems and methods

Materials & experimental systems

n/a	Involved in the study
<input type="checkbox"/>	<input checked="" type="checkbox"/> Unique biological materials
<input type="checkbox"/>	<input checked="" type="checkbox"/> Antibodies
<input checked="" type="checkbox"/>	<input type="checkbox"/> Eukaryotic cell lines
<input checked="" type="checkbox"/>	<input type="checkbox"/> Palaeontology
<input checked="" type="checkbox"/>	<input type="checkbox"/> Animals and other organisms
<input checked="" type="checkbox"/>	<input type="checkbox"/> Human research participants

Methods

n/a	Involved in the study
<input checked="" type="checkbox"/>	<input type="checkbox"/> ChIP-seq
<input checked="" type="checkbox"/>	<input type="checkbox"/> Flow cytometry
<input checked="" type="checkbox"/>	<input type="checkbox"/> MRI-based neuroimaging

Unique biological materials

Policy information about [availability of materials](#)

Obtaining unique materials All unique materials used are readily available from the authors.

Antibodies

Antibodies used

anti-GFP antibody (for Co-IP, Rohce,11814460001) (dilution volume, 1:1000);
anti-trimethyl-H3K36 antibody (for ChIP, Abcam,ab9050) (dilution volume, 1:200);
anti-HA antibody (for Co-IP, Rohce,11867431001) (dilution volume, 1:1000);
HA isolation kit (for Co-IP, MACS Miltenyi Biotec,130-091-122)

Validation

All antibodies were tested with controls. anti-trimethyl-H3K36 antibody was validated in Arabidopsis thaliana.